Neuron, Volume *96*

Supplemental Information

Active Mechanisms of Vibration Encoding and Frequency Filtering in Central Mechanosensory Neurons

Anthony W. Azevedo and Rachel I. Wilson

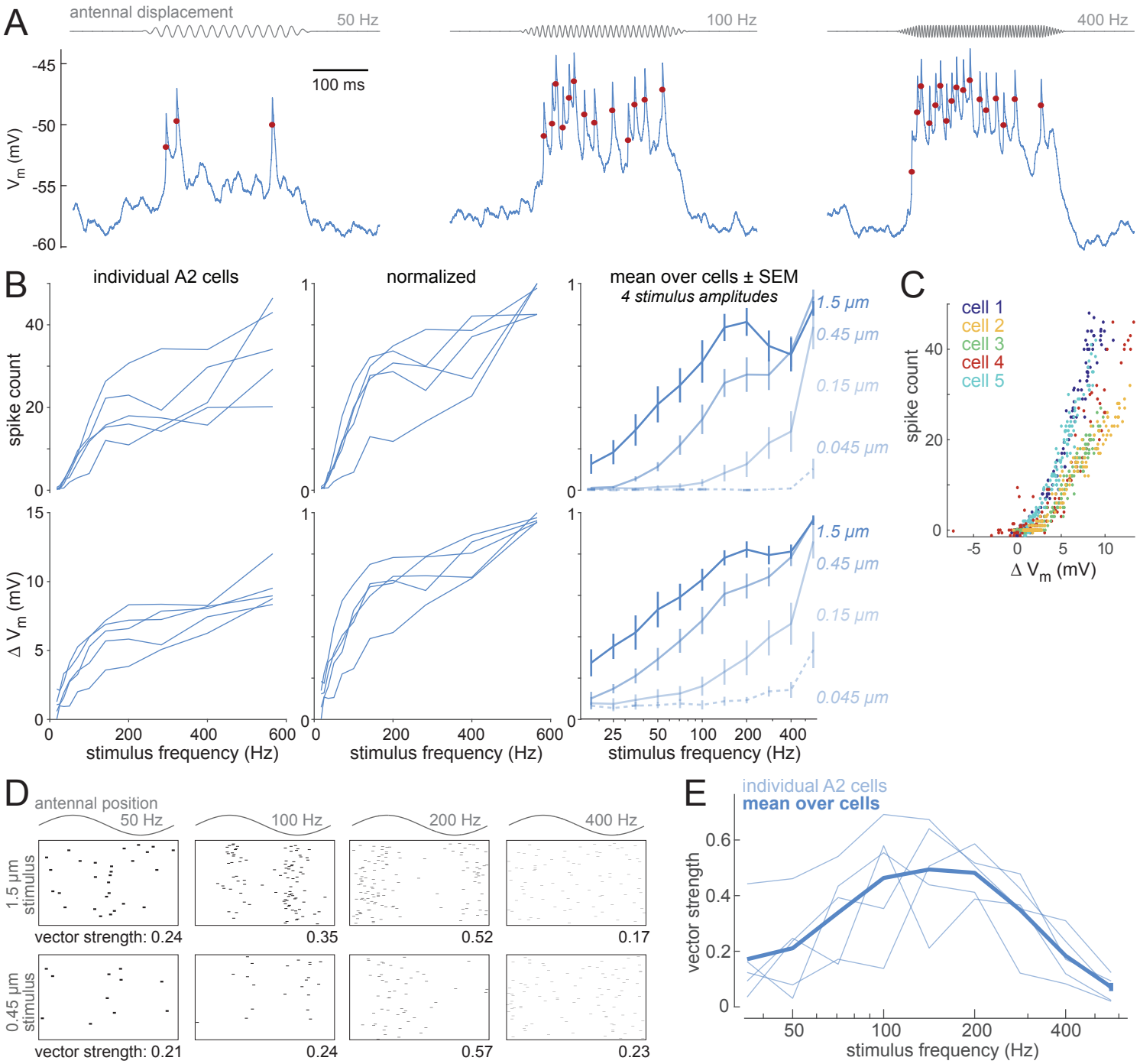

Figure S1, related to Figure 1: A2 cell spiking responses to vibration stimuli.

(A) Spikes in A2 cells (traces from Figure 1D). Spike onset is indicated with a red dot.

(B) Spiking responses (top) versus voltage responses (bottom, cells from Figure 2A). Spike count and ΔV were computed over the 300-ms stimulus presentation. For individual cell traces (left and middle columns), the stimulus amplitude was 0.45 µm. All A2 cells were recorded in the genotype *20XUAS-mCD8:GFP/+;VT30609-Gal4/+.*

(C) Spike count versus ΔV for all stimulus frequencies and amplitudes. Each point represents a trial. Spike count grows linearly with ΔV above the spike threshold.

(D) Rasters showing spike timing in a typical A2 cell for four stimulus frequencies and two stimulus amplitudes, 1.5 µm and 0.45 µm. Spikes are aggregated across all cycles and trials, with time normalized to stimulus period. A vector strength of 1 indicates all spikes occur at the same phase relative to the stimulus, whereas 0 indicates no phase preference.

(E) Vector strength for the highest stimulus amplitude (1.5 µm). Frequencies <35 Hz are omitted because the number of spikes was so low that the vector strength metric is not meaningful. For a typical cell, statistically-significant phase-locking (see Methods) was observed for the 200 Hz stimulus at the highest stimulus intensity. For some cells, significant phase-locking was also observed for other frequencies and amplitudes, but this was not reliable across cells.

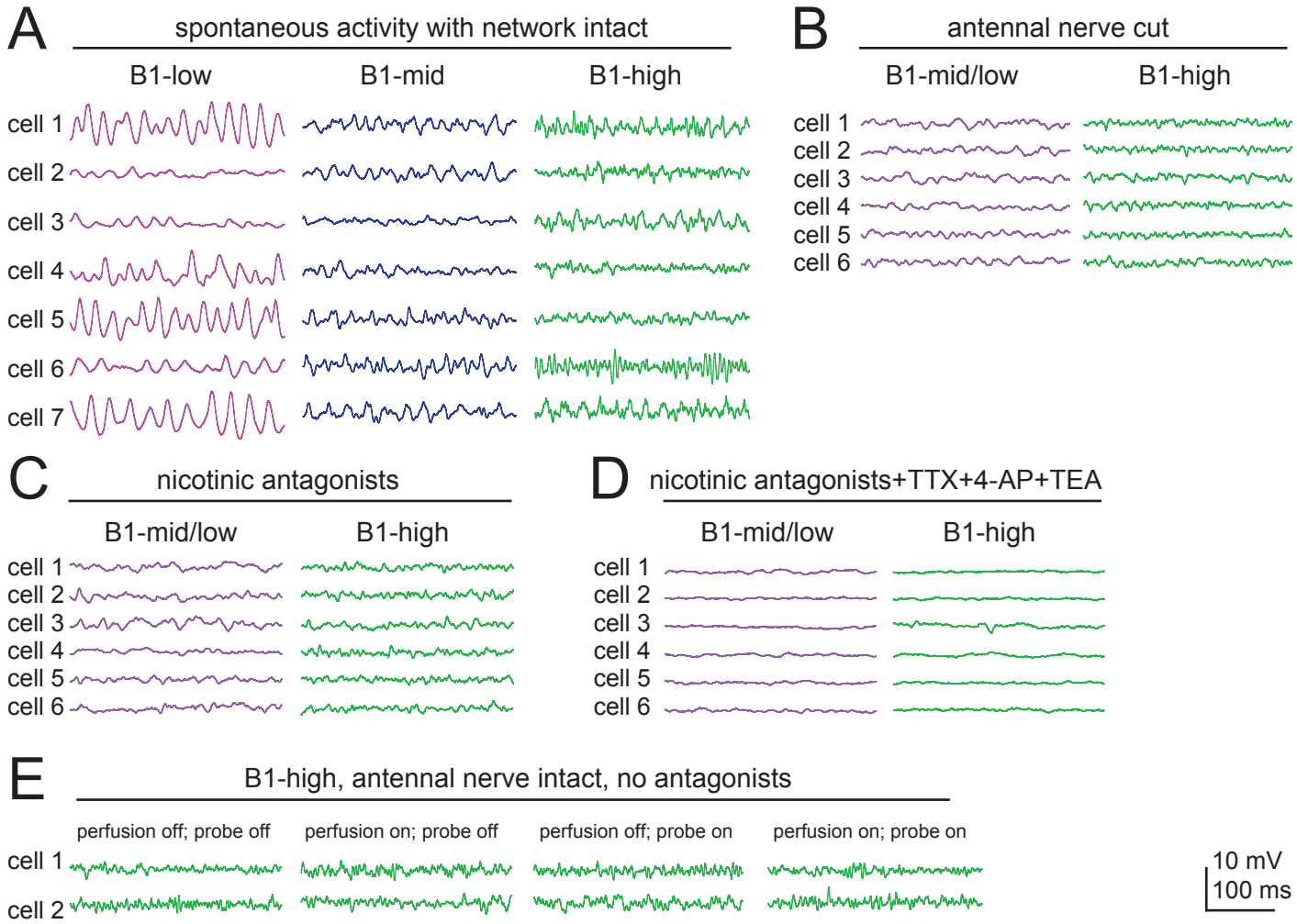

Figure S2, related to Figure 1: "Resting" oscillations in B1 cell voltage.

(A) Representative voltage recordings from seven B1 cells of each type. The antennal nerve was intact and there were no antagonists in the bath. The piezoelectric probe was attached to the antenna, and perfusion was flowed across the preparation, as in our standard experimental configuration, but no probe movement was commanded. Some cells showed oscillations under these conditions. Oscillations were generally largest and slowest in B1-low cells.

(B) Recordings with the antennal nerve cut. (Here we cannot distinguish B1-mid from B1-low because we do not have a Gal4 line which selectively labels either of these types.) Cutting the nerve greatly attenuates voltage fluctuations, indicating that these fluctuations are driven mainly by JON input.

(C) Adding nicotinic antagonists (after the nerve has been cut) has little effect.

(D) Blocking voltage-gated channels (with TTX/4-AP/TEA) further reduces the remaining fluctuations. The small effect of these drugs suggests that some periodic small fluctuations can arise as a result of cell-intrinsic mechanisms.

(E) Two B1-high cells were monitored before perfusion was turned on and before the probe was attached. Next, perfusion was turned on. Then, perfusion was turned off and the probe was attached. Finally, perfusion was turned on again. There was no clear effect of either perfusion or probe attachment in either cell. This implies that "resting" oscillations do not arise primarily due to perfusion-induced movements or spontaneous probe vibration.

To summarize, "resting" oscillations in B1 cells are mainly driven by JONs, and they are not primarily due to probe movement or perfusion-induced movement. Rather, they likely result from normal processes which are internal to the antenna. The a3 antennal segment can exhibit oscillatory movements at rest (Göpfert et al., 2005), and although a3 does *not* move measurably when the piezoelectric probe is glued to the arista, the same processes which normally drive a3 oscillations may still be creating oscillations in the tension on JON dendrites. Voltage-gated channels can create small fluctuations in the absence of synaptic input, but they are not the main source of "resting" oscillations.

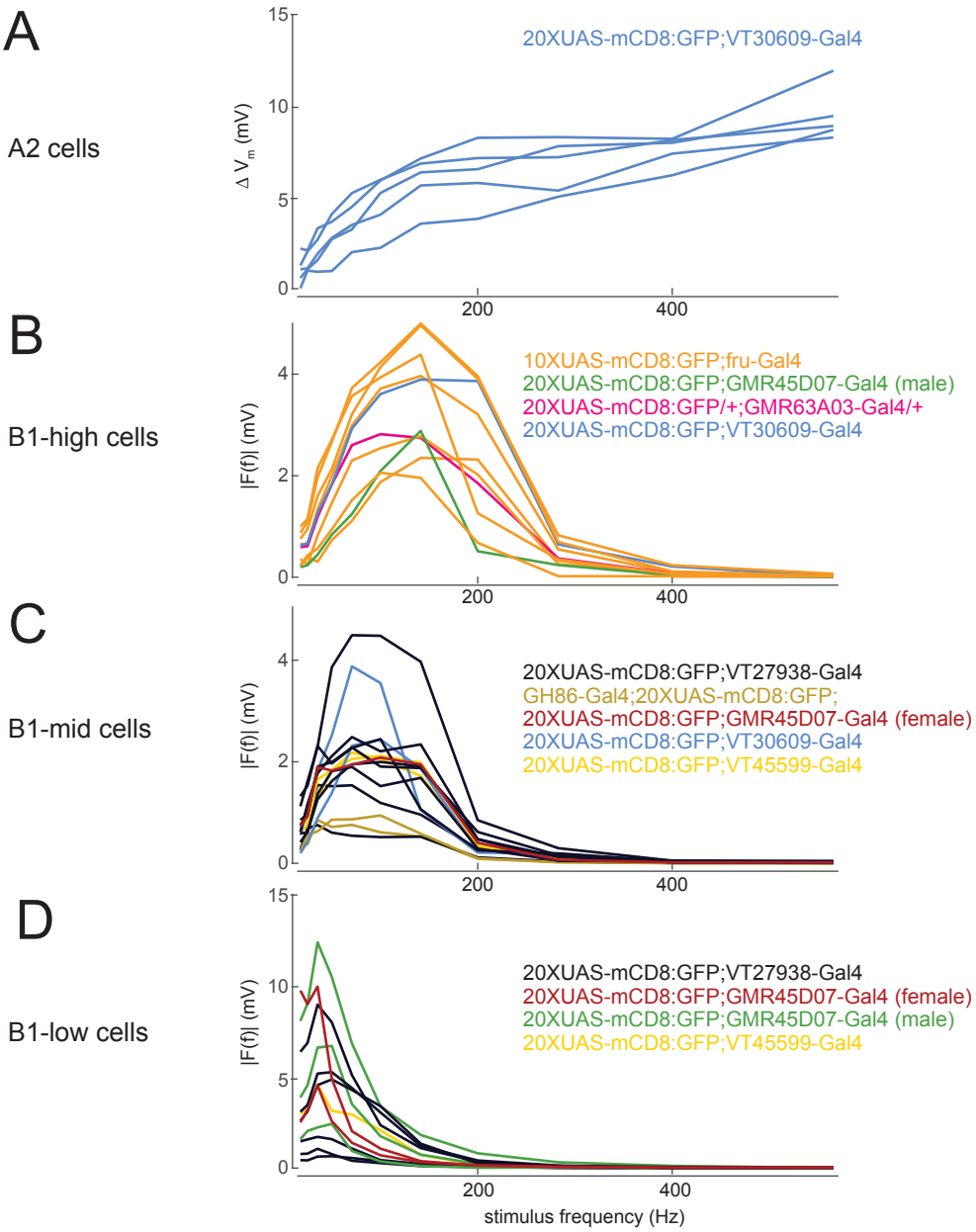

Figure S3, related to Figure 2: Gal4 lines labeling cells of different types.

(A) Tuning curves for A2 cells, reproduced from Figure 2A. Among the Gal4 lines we examined, only VT30609-Gal4 contained A2 cells.

(B) Tuning curves for B1-high cells, reproduced from Figure 2B. Cells are color-coded according to the Gal4 line in which they were found.

(C) Same for B1-mid cells, reproduced from Figure 2C.

(D) Same for B1-low cells, reproduced from Figure 2D.

Note that cells were classified on the basis of their intrinsic properties, and not just on the basis of the turning curves shown here (see Methods). Note also that we encountered only B1-high cells in fru-Gal4, and we encountered only B1-mid/low cells in VT27938-Gal4. We therefore used these two lines to specifically target either B1-high cells or B1-mid/low cells in voltage clamp experiments (Figure 5, Figure 7, Figure 8). Taking the data in this study as a whole, we found each B1 cell type in the following Gal4 lines:

B1-high cells: fru-Gal4, GH86-Gal4, VT30609-Gal4, GMR63A03-Gal4, and GMR45D07-Gal4
B1-mid cells: VT27938-Gal4, GH86-Gal4, VT30609-Gal4, VT45599-Gal4, and GMR45D07-Gal4
B1-low cells: VT27938-Gal4, GH86-Gal4, VT45599-Gal4, and GMR45D07-Gal4

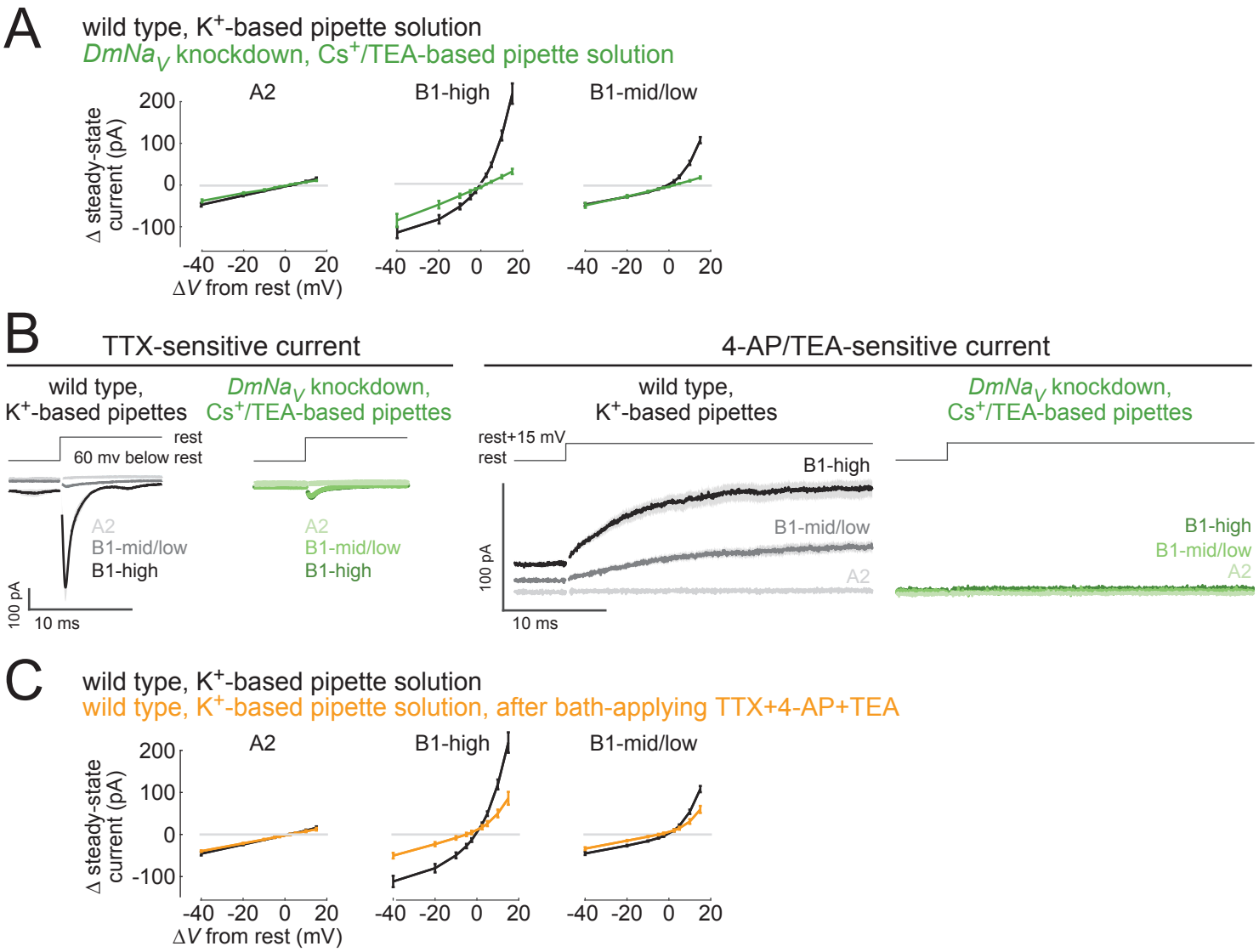

Figure S4, related to Figure 5: Suppressing voltage-gated conductances.

(A) Steady-state current-voltage curves (mean ± SEM across cells). Black: wild type genotype with K+-based pipette solution (n = 5 A2 cells, 8 B1-high cells, 7 B1-mid/low cells). Green: *DmNa*$_V$ knockdown genotype with Cs+/TEA internal (n = 5 A2 cells, 7 B1-high cells, 7 B1-mid/low cells). *DmNa*$_V$ knockdown should block voltage-gated Na+ currents, whereas Cs^+/TEA should block K^+ currents. As expected, the green curves are almost completely linear, supporting the idea that almost all voltage-dependent conductance has been blocked as a result of these combined manipulations. In this setting, the currents we record in response to mechanosensory stimuli should be relatively pure synaptic currents, with little or no contribution from voltage-gated conductances (see Figure 5). Voltages are relative to rest (-40, -20, -10, -5, -2.5, 2.5, 5, 10, and 15 mV).

(B) Transient currents. Left: TTX-sensitive current. Right: 4-AP/TEA-sensitive current. Traces represent mean ± SEM across cells. TTX-sensitive transient current was measured at the offset of a hyperpolarizing step command (a step starting -60 mV below rest and then jumping back up to the resting potential). Note that B1-high cells have especially large TTX-sensitive transient currents. Right: 4-AP+TEA-sensitive current during a depolarizing step command (a step starting at rest and jumping to 15 mV above rest). Note that B1-high cells have the largest 4-AP+TEA-sensitive current. In the *DmNa*$_V$ knockdown genotype with Cs+/TEA internal, the TTX-sensitive current is almost completely eliminated, as is the 4-AP/TEA-sensitive current.

(C) Steady-state current-voltage curves (mean ± SEM across cells) in the wild type genotype with K^+-based pipette solution. Black: same data in panel (A) above. Orange: after bath-applying TTX, 4-AP, and TEA in the same cells, these curves are more linear, meaning that much (but not all) of the total voltage-dependent conductance has been blocked. These are the same experiments shown in Figure 7B-C.

Genotypes: wild type - same genotypes as in Figures 7-8 (see Methods)
DmNa$_V$ knockdown - (A2): UAS-dcr2;20XUAS-CD8:GFP/+;VT30609-Gal4/UAS-DmNa$_V$-IR
(B1-high): UAS-dcr2;10XUAS-CD8:GFP/+;fru-Gal4/UAS-DmNa$_V$-IR
(B1-mid/low): UAS-dcr2;20XUAS-CD8:GFP/+;VT27938-Gal4/UAS-DmNa$_V$-IR

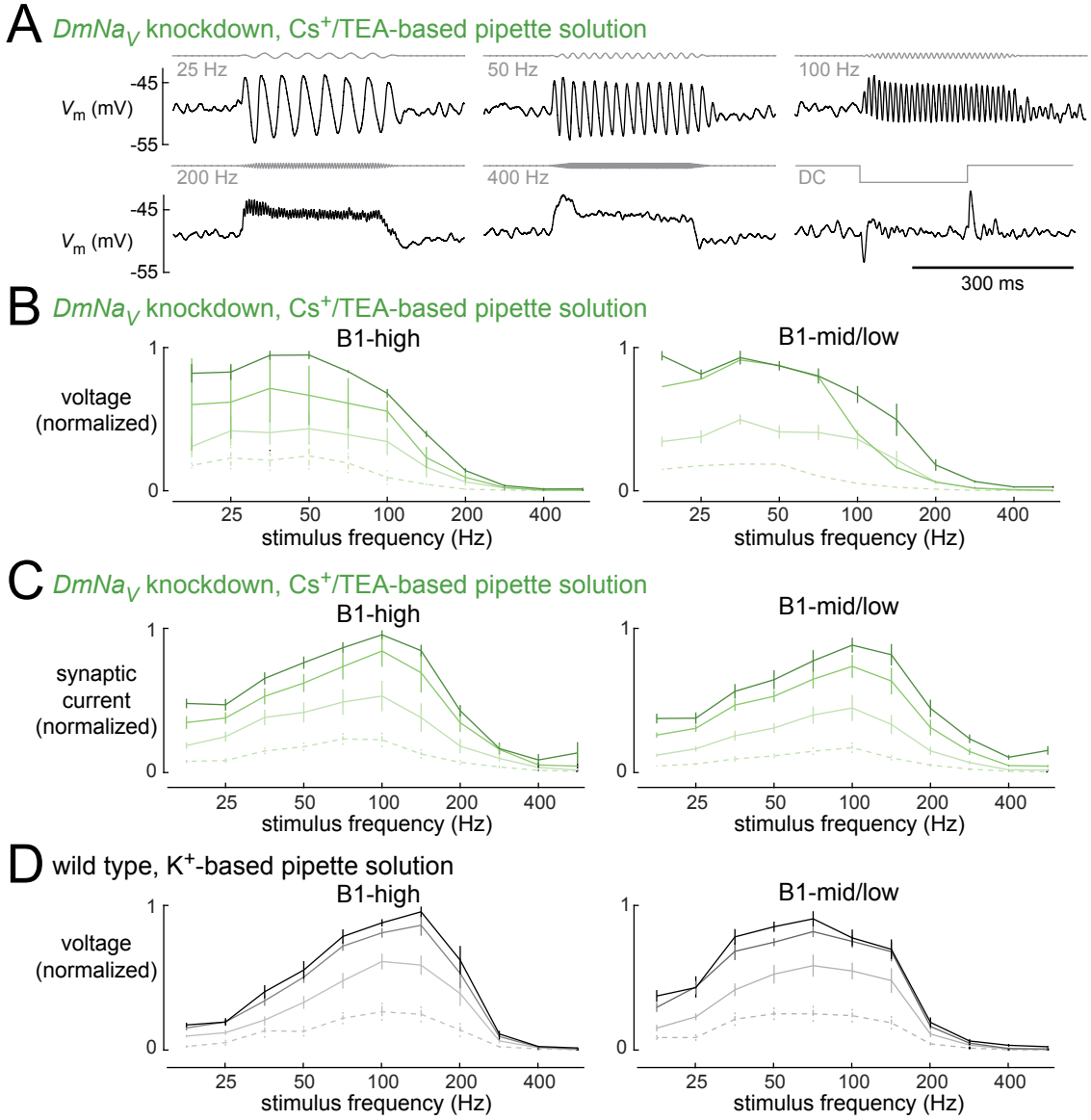

Figure S5, related to Figure 5: Blocking voltage-gated channels creates low-pass voltage tuning in B1 cells.

(A) Stimulus-evoked voltage responses in an example B1-high cell where *DmNa$_V$* expression has been knocked down, and where K^+ channels are blocked by Cs^+/TEA in the pipette solution. Stimulus amplitudes are 1.5 µm (vibrations) and -3 µm (steps). Traces are trial-averaged. Note that voltage responses are low-pass tuned. This contrasts with the normal situation, where voltage responses are bandpass tuned. (Compare this B1-high cell with the cell in Figure 1G, which is also B1-high, but recorded in a wild type fly with a K^+-based pipette solution that leaves voltage-gated conductances intact.) Note also the DC depolarization in response to high-frequency vibrations (e.g., 400 Hz); this DC depolarization reflects the small net inward synaptic current (Figure 5A) which is normally suppressed by voltage-gated conductances. Genotype is *UAS-dcr2/+;10XUAS-CD8:GFP/+;fru-Gal4/UAS-DmNaV-IR.*

(B) Data from all such experiments (mean ± SEM across cells, n = 7 B1-high, n = 7 B1-mid/low, not all cells tested with every stimulus amplitude). Stimulus amplitudes are 0.045, 0.15, 0.45, and 1.5 µm. The response is the magnitude of the Fourier component at the stimulus frequency. Note low-pass tuning, in contrast to the normal voltage responses of B1 cells, which are bandpass tuned; compare with (d) below. Genotypes are the same as for Figure 5 B1 cell data (**B1-high** is *UAS-dcr2/+;10XUAS-CD8:GFP/+;**fru-Gal4**/UAS-DmNaV-IR*, **B1-mid/low** is *UAS-dcr2/+;20XUAS-CD8:GFP/+;**VT27938-Gal4**/UAS-DmNaV-IR*).

(C) Synaptic currents in the same experiments are bandpass tuned (reproduced from Figure 5C). Passive membrane properties would be expected to low-pass filter these synaptic currents, and so it makes sense that the voltage responses in these cells would be low-pass, given that voltage-gated conductances have been essentially eliminated by knockdown of voltage-gated Na^+ channels and pharmacological blockade of voltage-gated K^+ channels.

(D) With voltage-gated conductances intact (in wild type flies with K^+-based pipette solution), voltage responses are bandpass tuned. Compare with (B). Data are reproduced from Figure 2, but to make a direct comparison with (A-C) we include here only those B1 cells recorded in *fru-Gal4* (B1-high, n=7) or *VT27938-Gal4* (B1-mid/low, n=14).

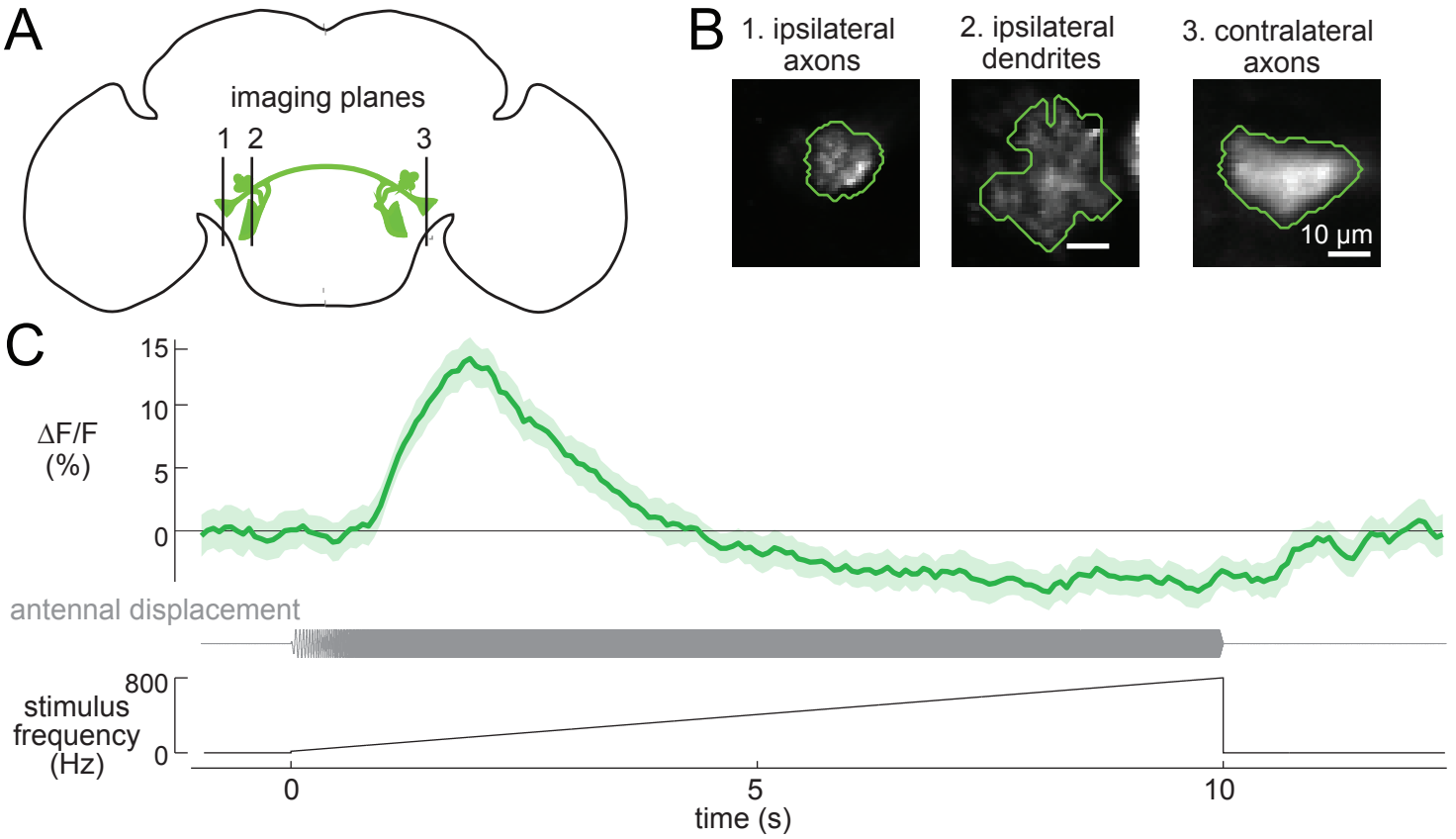

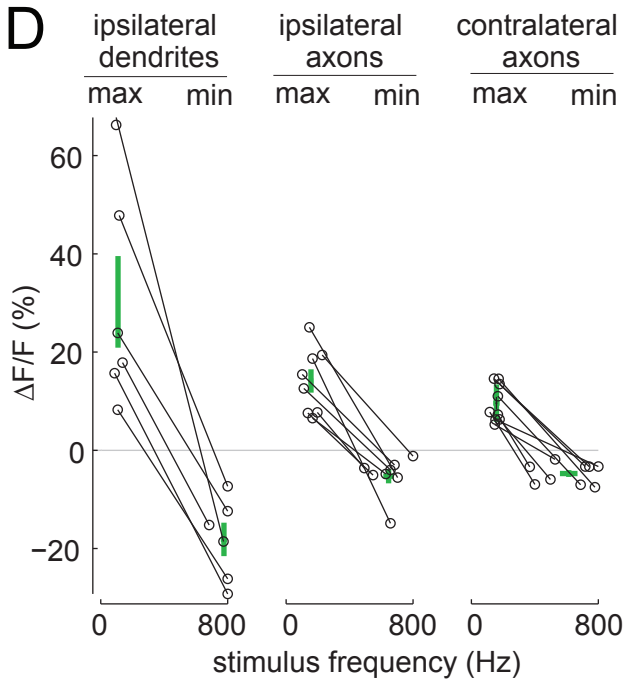

Figure S6, related to Figure 6: *In vivo* calcium imaging in B1 cells.

(A) Imaging planes targeting B1 axons and dendrites, centered on [1] ipsilateral axon terminals in the wedge, [2] ipsilateral dendrites in the AMMC, and [3] contralateral terminals in the wedge. Ipsi/contra are relative to the stimulated antenna.

(B) Typical resting fluorescence in each plane. Fluorescence is averaged within indicated regions of interest. Genotype is *20XUAS-GCaMP6s/+;GMR45D07-Gal4/+*.

(C) Response of contralateral axon terminals in a typical experiment (n=4 trials, mean ± SEM). The stimulus is a frequency sweep from 3 to 800 Hz. (When the stimulus was reversed, from 800 Hz to 3 Hz, the fluorescence decreased initially, and then increased at frequencies near 200 Hz.) In B1 cells, ΔF/F values are relatively small, which may reflect the fact that B1 cells are depolarized and hyperpolarized by each sound cycle, and so the net change in voltage is near zero. Calcium imaging averages across individual cycles, and so the positive and negative parts of the response tend to cancel out, yielding a small change in fluorescence.

(D) Maximum and minimum ΔF/F for each imaging plane in each experiment, taken from trial-averaged responses as in panel (C), and plotted versus the corresponding stimulus frequency. Two frequencies are shown for each experiment. Green lines are mean ± SEM (with error bars in both dimensions). Responses in axons are about half as big as responses in dendrites, which is not unexpected, given that voltage signals may be filtered as they move from dendrites to axon, and calcium permeability may be different in axons versus dendrites. The fact that ipsilateral signals are somewhat larger than contralateral signals is likely due to the fact that axon terminals are typically larger on the ipsilateral side.

In summary, these experiments confirm that stimulus-evoked signals do propagate successfully into both ipsi- and contralateral axon arbors, and the size of these axonal signals is reasonable, even though B1 cells do not spike.

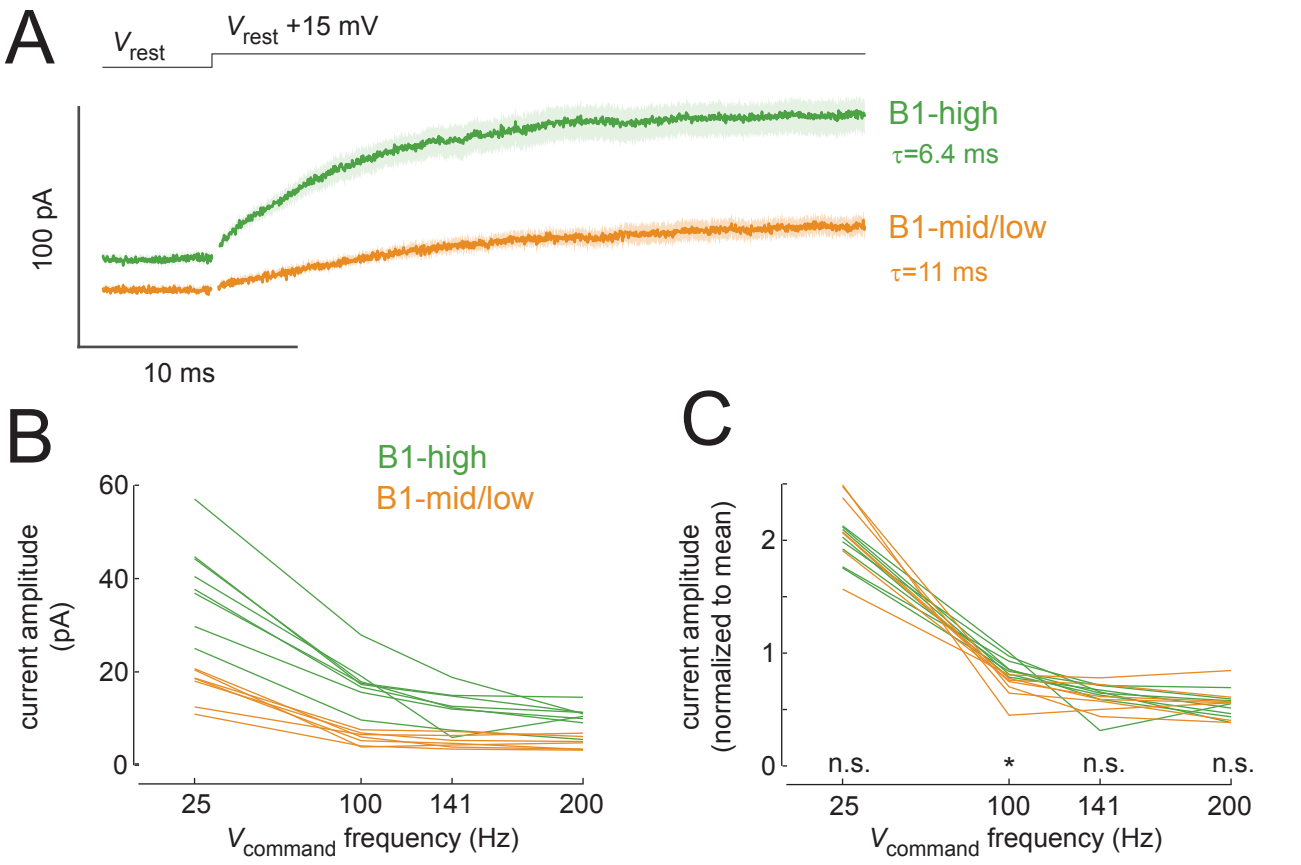

Figure S7, related to Figure 7: Voltage-gated K^+ currents are faster in B1-high cells than in B1-mid/low cells.

(A) 4-AP+TEA-sensitive current evoked by depolarizing voltage step commands, as in Figure 7 (mean ± SEM across cells, data reproduced from Figure S4B). An exponential function fit to the first 60 ms of the mean current yields a time constant (τ) which is smaller for B1-high cells than for B1-mid/low cells. Fitting data from individual cells yields a statistically significant difference between values of τ for B1-high cells versus B1-mid/low cells ($p = 0.0022$, ranksum test).

(B) 4-AP+TEA-sensitive current evoked by sinusoidal voltage commands (same experiments as in Figure 8). For all stmulus frequencies, there is more current in B1-high cells than in B1-mid/low cells. However, there is also a difference in the frequency-dependence of the current amplitude, which is easier to see when these curves are normalized. Each line is a different experiment.

(C) Same data normalized to the mean current in each cell across all four stimulus frequencies. Overall, the shapes of the normalized curves are similar, but there is a significant difference between B1-high and B1-mid/low for the 100 Hz stimulus (ranksum test with Bonferroni-Holm correction, m=4 tests, $p=0.0006$). This means that the voltage-gated K^+ current in B1-mid/low cells decays more steeply as voltage oscillation frequency increases 25 Hz to 100 Hz, whereas this current does not decay as steeply in B1-mid/low cells. The voltage-gated K^+ current opposes the voltage response to synaptic currents at this frequency, so this kinetic difference helps explain why B1-high cells typically prefer our 141 Hz stimulus, whereas B1-mid/low cells typically prefer lower-frequency stimuli.

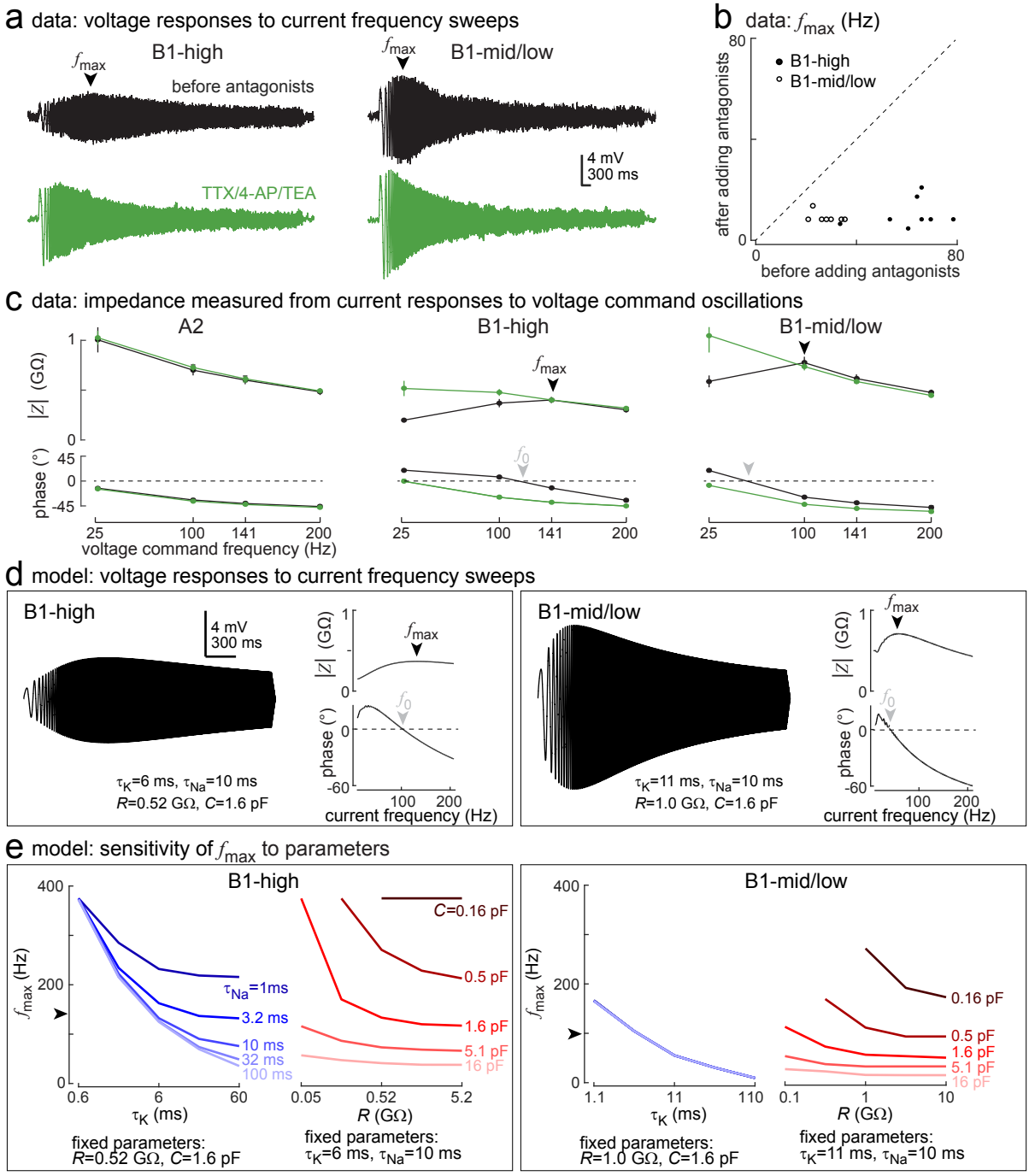

Figure S8, related to Figure 8: Frequency selectivity in B1 cells and comparisons with models.

(A) Example B1 cell voltage responses to current frequency sweeps (10 pA amplitude, swept from 0.3 to 300 Hz, mean of 4 trials). Spindle-shaped responses indicate bandpass tuning. TTX/4-AP/TEA suppressed responses to high frequencies.

(B) Summary of all experiments with current frequency sweeps, showing f_{max} before and after adding TTX/4-AP/TEA. These are the cells shown in Figure 8A-B (8 B1-high cells, 7 B1-mid/low cells). Note that f_{max} values are lower than in Figure 8C because model cells have a single compartment (no cable filtering). In real cells recorded in current-clamp mode, cable filtering will attenuate voltages as they propagate between the soma and the rest of the cell, thereby reducing the contributions of voltage-gated conductances in distant compartments.

(C) Impedance (from data in Figure 8A-B). Impedance has both magnitude (|Z|, top) and phase (bottom). For B1 cells, adding TTX/4-AP/TEA increases impedance at low frequencies. The frequency where current switches from lagging to leading (f_0) is the point where capacitive currents (leading) balance voltage-gated currents (lagging). Note that f_{max} values are higher than in panel (A), although the cells are the same; this reflects the contribution of cable filtering to (A).

(D) Modeled voltage responses to current frequency sweeps (10 pA, 0.3 to 400 Hz). Arrowheads show f_{max} and f_0 for model cells. Note good agreement with voltage clamp data in panel (C) and Figure 8A-B. See Methods for details.

(E) Sensitivity of f_{max} to model parameters (τ_K, τ_{Na}, R, C). Arrowheads show f_{max} from data in panel (C). Omitted values indicate an unstable model. Note that f_{max} changed smoothly with model parameters, and it was sensitive to all parameters (except τ_{Na} in the B1-mid/low model, because g_{Na} is nearly voltage- independent in B1-mid-low; Figure 7B-C).